ACADEMIC PRESS

Available online at www.sciencedirect.com
SCIENCE DIRECT®

NeuroImage 20 (2003) 995–1005

NeuroImage

www.elsevier.com/locate/ynimg

Determination of activation areas in the human auditory cortex by means of synthetic aperture magnetometry

Anthony T. Herdman,[a] Andreas Wollbrink,[a,b] Wilkin Chau,[a] Ryouhei Ishii,[a,c] Bernhard Ross,[a,b] and Christo Pantev[a,b,*]

[a] *Rotman Research Institute, Baycrest Centre for Geriatric Care, University of Toronto, Toronto, Canada M6A 2E1*
[b] *Institute for Biomagnetism and Biosignalanalysis, Münster University Hospital, Münster, Germany*
[c] *Department of Post-Genomics and Diseases, Division of Psychiatry and Behavioral Proteomics, Osaka University, Osaka 565-0871, Japan*

Received 17 April 2003; revised 13 June 2003; accepted 30 June 2003

Abstract

In this study we applied synthetic aperture magnetometry (SAM) to investigate active cortical areas associated with magnetically recorded transient and steady-state auditory evoked responses. For transient evoked responses, SAM images reveal an activated volume of cortical tissue within the lateral aspect of the superior temporal plane. The volume of cortical activation for steady-state responses was located more medially than that for transient evoked responses. Additionally, SAM also reveals a small overlap of activated areas between transient and steady-state evoked responses, which has not be demonstrated when using equivalent current dipole (ECD) source modeling. Source waveforms from SAM and ECD analyses show comparable temporal information. Results from this study suggest that SAM is a useful technique for imaging cortical structures involved in processing perceptual information.

Keywords: Synthetic aperture magnetometry (SAM); Transient and steady-state auditory evoked fields; Dipole source modelling; Magnetoencephalography

Introduction

Several studies have investigated the origins of auditory evoked responses (AERs) in humans using electroencephalography (EEG)(for reviews see Eggermont and Ponton, 2002; Naatanen and Picton, 1987) or magnetoencephalography (MEG)(for review see Jacobson, 1994). A negative electric wave peaking at approximately 100 ms in a vertex recording, referred to as N1 (Picton et al., 1974), is the one of the most robust components of the transient AER. The electrically recorded N1 consists of two sources located in the superior temporal gyrus, a main dipolar source that is tangentially oriented to the surface of the scalp and a second dipolar source that is radially oriented (Scherg and von Cramon, 1985). In contrast, magnetic recordings are sensitive mostly to tangential sources, thus the source of the magnetic counterpart of N1 (N1m) is equal to that for the principal contributor to the electric N1 (see Jacobson, 1994). Several MEG studies coregister the subject's MRI to the head shape model used in dipole source modeling and reveal that the N1m dipole is situated in the lateral aspect of the transverse temporal gyrus (Kanno et al., 2001; Pantev, 1995; Pantev et al., 1991b, 1995; Reite et al., 1994; Yamamoto et al., 1988). These EEG and MEG studies provide comparable results to those from animal studies and human studies using intracerebral electrodes (for reviews see Jacobson, 1994; Naatanen and Picton, 1987).

Another auditory response that can be evoked in the auditory modality is the steady-state evoked response (SSRs). SSRs can be elicited by regularly repeating auditory stimuli (Galambos et al., 1981) or amplitude-modulated tones (Cohen et al., 1991). Herdman et al., 2002) reported that the electrically recorded 40-Hz SSRs are mainly generated from a tangentially oriented source within the audi-

* Corresponding author. Rotman Research Institute, Baycrest Centre for Geriatric Care, Canada Research Chair "Human Cortical Plasticity," University of Toronto, 3560 Bathurst Street, Toronto, Ontario, Canada M6A 2E1. Fax: 416-785-2862.
E-mail address: pantev@rotman-baycrest.on.ca (C. Pantev).

1053-8119/$ – see front matter © 2003 Elsevier Inc. All rights reserved.
doi:10.1016/S1053-8119(03)00403-8

tory cortex. They showed that there is little contribution from radially oriented cortical sources, thus magnetic recordings will pick up most of the 40-Hz SSR. A number of MEG studies have localized the source of the magnetic SSR to be within the superior temporal plane (Gutschalk et al., 1999; Hari et al., 1989; Makela and Hari, 1987; Pantev et al., 1996). By superimposing the SSR dipolar sources onto the corresponding MRI, Pantev et al. (1996) showed that SSRs are generated within the primary auditory cortex (i.e., the medial portion of transverse temporal gyrus). Compared to the N1m source location, the SSR generators are more medially located (Hari et al., 1989; Pantev et al., 1993). This demonstrates that the centers of gravity for activated areas are significantly different; however, the extent to which these cortical regions overlap was not determined. This volumetric overlap is difficult to establish in these studies because of the constraints and assumptions necessary for equivalent current dipole (ECD) source modeling.

Methods such as functional magnetic resonance imaging (fMRI) or positron emission tomography (PET) are capable of spatially resolving the brain volumetric area activated by acoustic input (Belin et al., 1999; Johnsrude et al., 2002; Lockwood et al., 1999; Pastor et al., 2002; Scheffler et al., 1998; Talavage et al., 2000; Wessinger et al., 1997). Most of these studies show activated volumes that include the transverse temporal gyrus and the posterior-lateral aspect of the superior temporal gyrus. In a PET study, Lockwood et al. (1999) showed a broad area of activation that extends beyond the medial two-thirds of the transverse gyrus, as well as activated volumes within brainstem structures, to pure-tone stimuli. These results suggest that simple acoustic stimuli activate auditory regions beyond the primary auditory cortex (i.e., medial two-thirds of the transverse gyrus). This is supported by further evidence from fMRI studies by Belin et al. (1999) and Talavage et al. (2000). However, because of the poor temporal resolution, PET and fMRI cannot separate the brain regions that independently generate transient, sustained, and steady-state components of the complex auditory response. Thus, it is to be expected that the PET and fMRI results include all areas that are activated by an acoustic stimulus. In order to differentiate the multiple volumes of active tissue that are functionally separate, we need a method that can resolve these activated volumes in both space and time.

Synthetic aperture magnetometry (SAM) is a novel approach to analyzing MEG data (Ishii et al., 1999; Robinson and Vrba, 1998; Singh et al., 2002; Taniguchi et al., 2000). SAM analysis has the advantage of providing more temporal and spatial information than fMRI and ECD modeling, respectively. SAM can create images of several active brain regions with a spatial resolution that is similar to fMRI, but with much better temporal resolution (on the order of milliseconds). Compared to ECD analysis, SAM can identify the volume of activation rather than the center of gravity by using a spatial filtering method to identify separate volumes of tissue that are active for specific time periods in the MEG waveform. The SAM approach is data driven and does not use an inverse solution to calculate source activity. This means that SAM is not limited by many of the hypothetical constraints needed for ECD modeling. Nevertheless, SAM does have its own limitations. In order to reduce the noise in the signal, the spatial filter attenuates correlated activity between hemispheres for a given point in time (Van Veen et al., 1997).

In this study, magnetically recorded transient AERs and SSRs were elicited by long-duration amplitude-modulated tones. These two types of responses were chosen to test if SAM was sensitive enough to circumscribe their separate neural generators. For comparison, we used ECD modeling and compared the time course of active sources within the temporal lobes that were localized by means of SAM and ECD analyses.

Methods

Subjects

Thirteen subjects (seven females) with normal audiological status participated in this study. Subjects were between the ages of 24 and 50 years (mean age 33.3 years) and all were right-handed. Informed consent was obtained from each subject after the nature of the study was fully explained. This experiment was part of a larger project entitled "Magnetic Studies of Human Hearing," which had received approval from the Ethics Committee of the Baycrest Centre for Geriatric care. The subjects were paid for their participation.

Stimulation

Auditory stimuli consisted of sinusoidal 100% amplitude-modulated tone bursts having a modulation frequency of 40 Hz and a carrier frequency of 500 Hz. Each tone burst had a duration of 2.0 s with a rise and a fall time of 10 ms. Stimuli were presented binaurally at a randomized interstimulus interval of 2.0 ± 0.5 s. Seventy-five stimuli were presented in two separate blocks within one session. All auditory stimuli were delivered binaurally to silicon earpieces placed in the left and right ear using a nonmagnetic and echo-free acoustic delivery system. Individual hearing thresholds for the stimuli were determined to within 5 dB for both ears. The stimuli were presented at 60 dB SL (sensation level). Prior to the start of the experiment, both the signal spectrum and the correct timing of the stimulus were verified by measuring the output of the earphones using a sound-level meter.

Data acquisition

All recordings were done in a magnetically shielded room using a 151-channel whole-head biomagnetometer system (CTF Systems Inc.) with detection coils spaced by 31 mm. The sensors were configured as first-order gradiometers with a baseline of 50 mm. The spectral density of the intrinsic noise of each channel was about 5 fT/Hz^{-2} in the frequency range above 1 Hz.

Subjects were seated comfortably in an upright position with their back firmly supported by a vacuum cushion. Head movements were monitored using a head coil localization system. No head movements (greater than 8 mm) sufficient to require the discarding of data were observed (mean head movement during a session equaled 5.4 mm). Subjects were asked to remain alert and compliance was verified using a video monitor. In order to control for confounding changes in attention and vigilance, subjects watched a self-selected movie without accompanying sound presentation.

Stimulus-related epochs of 4.7 s duration (including a 0.2-s prestimulus interval) were recorded using a bandwidth of DC to 104 Hz and a sampling rate of 312.5 Hz. Magnetic field data elicited by 150 stimuli were recorded and stored for further analysis

Data analysis

Trials contaminated by muscle or eye blink artifacts were rejected from the averaging process. Rejection threshold was chosen after careful inspection of the individual data. Trials without artifacts were averaged and baseline corrected relative to the prestimulus interval. Analysis of the data concentrated on the transient and steady-state components of the auditory evoked response. The data were bandpass filtered in the range of 1–20 Hz for the transient and between 30 and 50 Hz for the steady-state responses.

ECD analyses

Source analyses, based on a spatiotemporal ECD model in a spherical volume conductor, were applied to the N1m component of the transient AER and to the SSR. For each subject, two ECDs (one in each hemisphere), defined by their moment, orientation, and spatial coordinates, were fit to five sample points (16 ms) around the N1m peak of the transient AER. For the SSR data, the real and imaginary parts from the fast Fourier transform of each sensor's signal were determined for the 40-Hz bin. A time function of a 40-Hz signal was calculated using these real and imaginary components. Two ECDs (one in each hemisphere) were fit to five sample points (16 ms) around the peak of the 40-Hz signal. Head models were coregistered to each subjects MRI for visual inspection (see Pantev et al., 1991a). For the transient N1m component and SSRs, one dipole was added to the left hemisphere and its position and orientation was fitted to the 16-ms time range. Then a second dipole was added to the right hemisphere and both dipoles were fitted to the same time window. Such dipole fitting had a high goodness-of-fit indicated by less than 10% residual variance of the field data. To determine differences in source locations, spatial coordinates for each ECD of the N1m and the SSR were averaged across subjects and their 95% confidence intervals were calculated.

The method called "source space projection" was used to collapse the time series of the MEG sensors (151 in our case) into a single waveform of the corresponding magnetic dipole moment. The relation defined by the following equation (Hamalainen et al., 1993):

$$b(r) = L(r,R) \times q(R) \tag{1}$$

mapped the current source $q(R)$ at the position R in the brain into a multidimensional *signal space* defined by the sensors at their positions r outside the head (Ilmoniemi et al., 1987). Each of these sensors measured a magnetic field $b(r)$. The lead-field matrix $L(r,R)$ depended on the properties of the volume conductor and the sensors and on the positions of the source and the sensors. To map the signal space into one or several current sources, a spatial filter was constructed. Therefore, the estimated orientation $q(R)/\imath qR\imath$ of the underlying source and the pseudoinverse of the lead-field matrix $L^{-1}(r,R)$ were used to calculate a weighting vector $W(q(R))$. The spatial filter was then defined as the dot product of measured magnetic field $b(t)$ and this weighting vector W (Robinson, 1989). The filter applied to the MEG data provided a single time-series waveform of the dipole moment that was seen by a virtual sensor located at the position of the current sources (Robinson and Rose, 1992). The method was spatially sensitive because the virtual sensor responded maximally to the region of interest in the brain. Contributions from other regions and uncorrelated system noise were reduced or respectively cancelled out.

SAM analyses

SAM is based on the concept of the beamforming technique commonly used in sonar and radar for signal detection. As an adaptive nonlinear beamformer, SAM applies a spatial filter, specific for each brain voxel, to suppress the interference of the unwanted signals (Robinson and Vrba, 1998). The spatial filter at location θ is a linear projection operator defined by a set of coefficients, with one coefficient for each sensor, which is determined by minimizing the source power. Statistical evaluation of the ratio of the power differences between the active and control windows to the sum of the powers of noise was expressed as a pseudo t value (T) for each voxel (θ) as follows:

$$T_\theta = \frac{S_\theta^{\mathrm{A}} - S_\theta^{\mathrm{C}}}{N_\theta^{\mathrm{A}} + N_\theta^{\mathrm{C}}}, \tag{2}$$

where S_θ^{A} and S_θ^{C} are the estimated power of the source for the active and control windows, respectively, and N_θ^{A} and N_θ^{C} are the estimated powers of the noise. For the transient AERs, the active and control windows were 0 to 0.25 s and -0.26 to -0.01 s with respect to the stimulus onset, respectively. For SSRs, the active and control windows were between 1 to 2 s and -1.1 to -0.1 s. We chose this later time window for the SSR because it has been shown (Ross et al., 2002) that the amplitude and phase of the 40-Hz response is constant from 250 ms after stimulus onset to stimulus offset. Because SAM greatly reduces correlated fields across hemispheres (Van Veen et al., 1997), SAM images were calculated for sensors in each hemisphere separately and then combined for visual display. Addition-

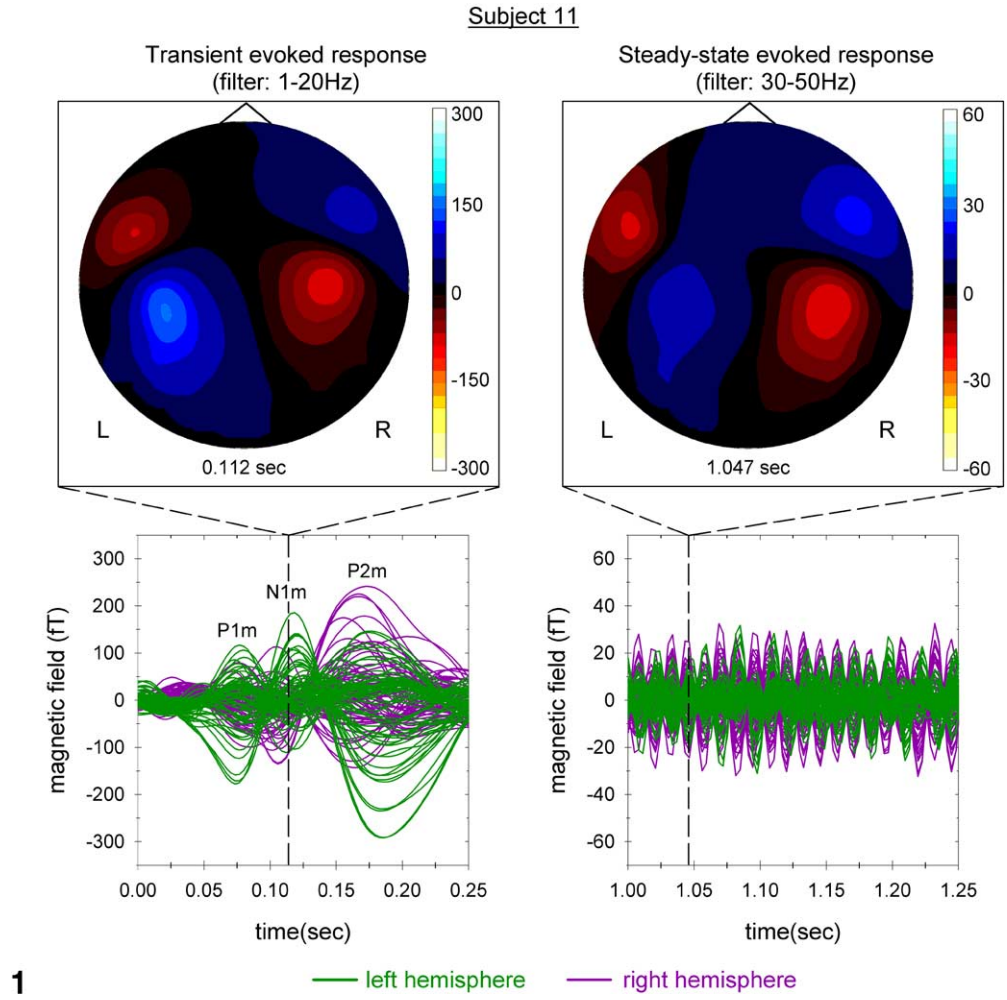

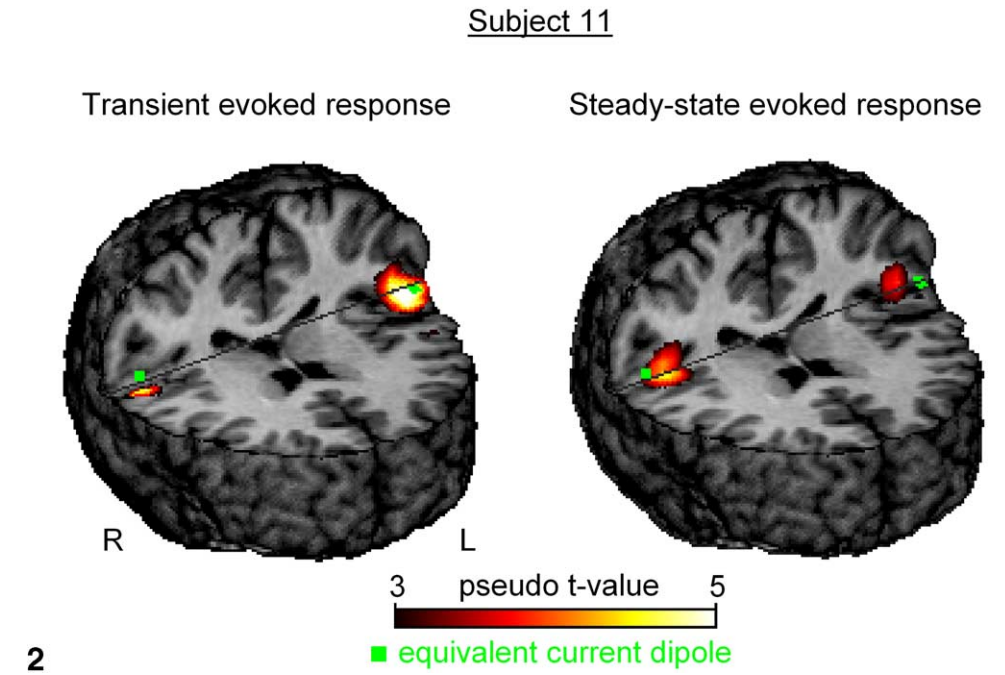

Fig. 1. Magnetic recordings of transient AERs and SSRs from a single subject. (Top) Field distributions from a top-view perspective with nose at top of figure. (Bottom) Fields from left- and right-hemisphere sensors graphed as a function of time. P1m, N1m, and P2m designate the first, second, and third peaks in the magnetic recording.

Fig. 2. A single subject's results from SAM and ECD analyses of the transient AERs and SSRs projected onto the subject's 3D brain. The frontal lobes have been removed to view the activated regions.

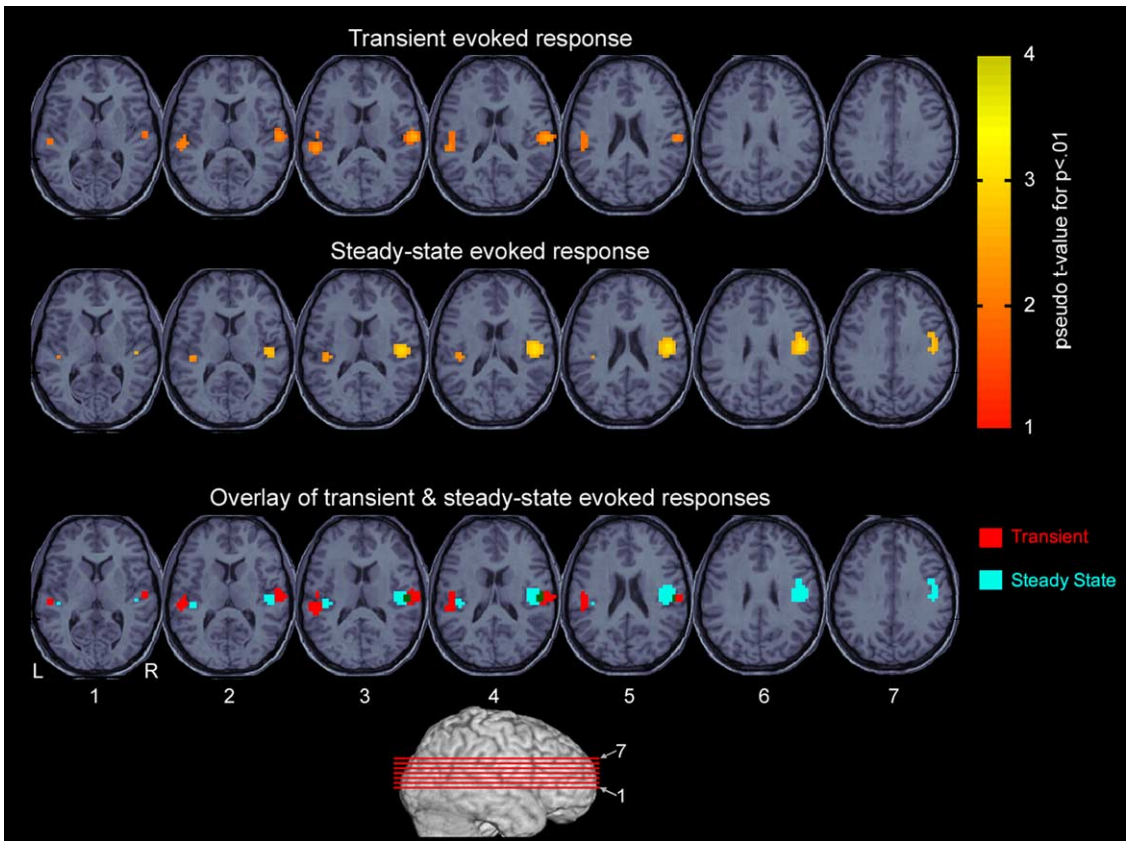

Fig. 3. Permutation results of SAM analyses for transient (top) and steady-state (middle) auditory evoked responses. Significant voxels are superimposed onto the structural MRI (5 mm axial slices; inferior–superior from left–right) as a function of the pseudo *t* value. Activation areas for transient AERs and SSRs show a small region of overlap depicted in green (bottom).

ally, the voxel location within each temporal lobe that had the maximal ("peak") pseudo *t* value was averaged across subjects and a 95% confidence interval was calculated.

To analyze the group data, it was necessary to transform each individual's data into a common anatomical space (Barnes and Hillebrand, 2003; Singh et al., 2002). This normalization step is a common procedure for the analysis of fMRI data. In this study, each subject's SAM images were converted to a common anatomical space using SPM99. Normalization of the data enabled us to perform a nonparametric statistic of each SAM voxel based on all the subjects' data and is classified as the "SAM permutation" statistic. The SAM permutation test determined which voxels are significant by comparing the grand mean pseudo *t* value of a voxel to a distribution of permuted pseudo *t* values. This distribution was computed by randomly rearranging the active and control conditions and averaging the newly calculated pseudo *t* values. The null hypothesis of SAM permutation is that the original grand mean pseudo *t* value falls within the permuted distribution of pseudo *t* values. The null hypothesis was accepted or rejected for each voxel at an α level of 0.01. Grand mean pseudo *t* values (T_θ) for significant voxels were then overlaid on a normalized structural MRI.

The time course of the source activity for a specific voxel can also be calculated using SAM. This is referred to as the SAM "virtual channel" and is conceptually similar to source space projection. A virtual channel is constructed for a specific point in space by applying weighting vectors, calculated from the beamformer's spatial filter, to the physical MEG sensors (Robinson and Rose, 1992). For each subject, a SAM virtual channel was determined separately for the transient AER and the SSR. The time windows used for transient AERs and SSRs were 0 to 0.25 s and 1 to 2 s, respectively. A SAM virtual channel was calculated at the voxel location in each temporal lobe that had the maximal pseudo *t* value. The SAM virtual channel waveforms were then averaged across subjects for both the transient AERs and SSRs.

Statistical analyses

From the individual source space projection waveforms, amplitudes for N1m component of the transient AERs were calculated as the maximal positive dipole moment within the latency range of 0.05 and 0.150 s. To determine a subject's source space projection amplitude for SSRs, a fast Fourier transform was used to determine the amplitude at 40 Hz. These individual source space amplitudes were then averaged across subjects. The same procedures used for calculating source space projection amplitudes were used for the SAM virtual channel data. A three-factor repeated-

measures analysis of variance (ANOVA) compared the amplitudes across two analyses (source space projection and SAM virtual channel), two response types (transient and SSR), and two hemispheres (left and right). Results of the ANOVA were considered significant if $P < 0.01$.

Bootstrap sampling distributions were calculated for the source space projection and the SAM virtual channel waveforms for each sample point across all subjects. The 95% confidence intervals (two-tailed) were determined for these sampling distributions and used as an estimate of the inter-individual variability within the data.

Results

Spatial domain

Topography

The topographies of magnetic fields for the N1m and 40-Hz SSR from a single subject are shown in Fig. 1. The peak of the N1m component (at 112 ms) has positive (outward) fields over the right frontal–temporal and left parietal–temporal regions and negative (inward) fields over the right frontal–temporal and left parietal–temporal regions (Fig. 1). The midpoints between the each hemispheres maxima and minima are located over the Sylvian fissure. The distribution of fields is similar for a peak in the 40-Hz SSR (at 1047 ms). However, the SSR fields are approximately six times smaller in amplitude as compared to the N1m fields.

SAM and ECD analyses

Figure 2 shows a single subject's results from SAM and ECD analyses of the transient AERs and SSRs superimposed onto the subject's 3D brain (reconstructed from MR images). The frontal lobes have been removed to view the regions of activation. SAM voxels are projected to the surface from a depth of 7 mm (i.e., from an adjacent slice). SAM results for the transient AERs show bilaterally localized activity around the lateral aspect of the superior temporal gyri, including the transverse temporal gyri. This active volume encompasses the location of the ECD in the left hemisphere, but is slightly inferior to the ECD in the right hemisphere. Comparing across hemispheres, there are higher pseudo *t* values and a broader region of activity in the left than the right. For SSRs, SAM results reveal bilaterally localized volumes of activity in the medial portion of the superior temporal gyri, including the transverse temporal gyri. The ECD location for the right hemisphere is in the lateral part of the SAM volume with high pseudo *t* values. In the left hemisphere, the ECD location is outside and lateral to the SAM volume with high pseudo *t* values. Note that for SAM analysis there are no other cortical regions with large pseudo *t* values. Results from the other 12 subjects' are consistent with those shown for subject 11, with the exception that the size of the SAM volumes and the magnitude of pseudo *t* values were variable between hemispheres. Five of the 13 and 3 of 13 subjects had SAM pseudo *t* values for SSRs that were less than 1.5 for the left and right hemispheres, respectively.

Figure 3 shows the permutation test results of the SAM images for the transient AERs and SSRs superimposed onto normalized axial MRI slices. Significantly active volumes for transient AERs are located bilaterally within the superior temporal plane. Greatest activity (high pseudo *t* value) is situated in the lateral aspect of the transverse gyri. For the SSRs, significantly active volumes are also located bilaterally within the superior temporal plane. High pseudo *t* values for SSR volumes overlap the medial aspect of the transverse gyri. Furthermore, there is a larger volume of significant voxels with higher pseudo *t* values for SSRs in the right as compared to the left hemispheres. Additionally, active volumes for SSRs are medial to those for transient AERs. Figure 3C displays the areas of significant voxels for the transient AERs and SSRs. Voxels that are significantly active for both transient AERs and SSRs are designated in dark green. This coactive region is bound medially by the SSR volume and laterally by the transient AER volume.

Figure 4 shows the median locations and 95% confidence intervals of the SAM peak pseudo *t* values for transient AERs and SSRs. The SAM peak pseudo *t* values for the transient AER are located in the lateral aspect of the transverse gyri. The SAM peak pseudo *t* values for SSRs lie near to the medial part of the transverse gyri. The transient AER SAM peak locations are, on average, more laterally situated as compared to the locations of SAM peak for SSRs by 1.26 and 1.17 cm in the left and right hemispheres, respectively. This difference is only significant in the right hemisphere, as indicated by nonoverlapping confidence intervals in the medial–lateral direction. The differences in locations for anterior–posterior and superior–inferior directions between transient AERs and SSRs did not reach significance, as indicated by their overlapping confidence intervals.

Figure 4 also shows for the left and the right hemisphere that the N1m dipoles are located slightly superior to the lateral aspect of the transverse gyrus. The median location of the ECDs for SSRs borders on the medial aspect of the transverse gyrus. Positions for the N1m ECDs are significantly more lateral to those for SSRs in both hemispheres, as indicated by their nonoverlapping confidence intervals. The mean differences between N1m and SSR ECD locations in the medial–lateral direction are 1.66 and 0.76 cm for the left and right hemispheres, respectively.

Furthermore, as compared to SAM peak pseudo *t* values, ECDs (averaged across transient AERs and SSRs) are 0.61 and 0.53 cm more laterally located in the left and right hemispheres, respectively. However, 95% confidence intervals overlap. Thus there are no significant differences in any direction of ECD locations for either transient AERs or SSRs as compared to SAM peak pseudo *t* value locations. The SSR confidence intervals for both SAM and ECD analyses are noticeably broader than the N1m confidence intervals, which indicate a larger variability in source locations across subjects.

Time domain

Field data

Figure 1 shows the plots of a single subject's MEG fields as a function of time for left and right hemispheric sensors. For transient AER fields, noticeable waves peak at approximately 70 ms (referred to as P1m), at 110 ms (referred to as N1m), and at 175 ms (referred to as P2m). Data from all subjects show this triphasic complex but with some variability in component amplitudes and latencies between subjects. The offset response also consists of this triphasic complex starting at approximately 70 ms after stimulus offset, although it smaller in amplitude as compared to the onset response. For the transient AERs of subject 11, the sensors over the left hemisphere measure fields that are larger than those over the right hemisphere. However, 6 of 13 subjects have larger transient AER fields measured over the right hemisphere than the left. There appear to be larger fields recorded over the right than the left hemisphere for SSRs of subject 11. However, 4 of 13 subjects have larger SSR fields measured over the left hemisphere than the right.

SAM virtual channel and source space projection

The source activity analyzed using SAM virtual channel and source space projection show similar time courses for either transient AERs or SSRs (Fig. 5). Because AERs are correlated and the spatial filtering technique of SAM removes correlated activity to reduce noise (Van Veen et al., 1997), SAM virtual channel waveforms represent uncorrelated source activity. This will be less than the source activity determined using source space projection. However, because the noise in the SAM virtual channel is also attenuated, the signal-to-noise ratios of the SAM virtual channel and source space projection are comparable. Thus, the scales for the SAM virtual channel plots are adjusted so that the maximal positive amplitude (e.g., N1m component of left hemisphere) matches the same level as the maximal source space projection amplitude (e.g., N1m component of the left hemisphere). This was done in order to remove the amplitude effect that obscures the visual comparison between the two measures. For the transient AERs (upper plots in Fig. 5), triphasic waveforms are noticeable in the 0.25 s window and represent the underlying source activity for the P1m-N1m-P2m complex as seen in the MEG field data. Only the 0.25 s window used for creating the SAM images is shown, because weighting functions for the SAM virtual channel would not be appropriate for determining the source strength outside of this window. For SSRs (lower plots in Fig. 5), 10 cycles are evident in the window between 1 and 1.25 s after stimulus onset. The right hemispheric SSR waveforms for the SAM virtual channel are noticeably larger than those for the left hemisphere. However, results from a three-factor ANOVA (analysis type $\times$ response type $\times$ hemisphere) reveal no significant difference ($P = 0.30$) in response amplitudes between hemispheres. Furthermore, the bootstrap-sampled 95% confidence intervals (thin lines in Fig. 5) of the source space projection and SAM virtual channel waveforms overlap between hemispheres.

Discussion

Spatial domain

Topography

The N1m component of the transient AER peaks at approximately 110 ms after stimulus onset and has a well-known distribution of magnetic fields over the scalp (Hari and Makela, 1986; Hari et al., 1987; Kanno et al., 2001; Makela and Hari, 1987; Pantev et al., 1993; Yamamoto et al., 1988). There is a minimum field over the right frontal–temporal region (magnetic flux out of the head) and a maximum field over the right parietal–temporal region (magnetic flux into the head). The pattern is reversed for the left hemisphere. This field topography is very similar to that for 40-Hz SSRs (Bertrand et al., 1991; Makela and Hari, 1987; Pantev et al., 1996; Romani, 1986), except that the SSR amplitudes are considerably smaller than those of N1m. Topographic results for the N1m and SSR from the present study are consistent with this familiar pattern.

SAM analyses

Our results demonstrate that SAM can be used to localize the cortical volumes involved in generating transient AERs, as well as SSRs. Moreover, SAM can successfully differentiate between them. In all subjects, the lateral aspect of the superior temporal gyrus was consistently activated in both hemispheres within the first 250 ms after a 40-Hz amplitude modulated tone was presented. In comparison to the cytoarchitecture of the auditory cortex, most subjects show an activated volume for the transient AERs to contain the lateral koniocortex (i.e., lateral aspect of Heschl's gyrus) and the internal and external parakoniocortices, as defined by Galaburda and Sanides, 1980). The SAM group permutation results clarify this consistency seen across subjects by illustrating that the same regions are included in the group image. The significantly active SAM volumes, as determined by the SAM permutation method, are comparable to previous reports using fMRI or PET (Belin et al., 1999; Johnsrude et al., 2002; Lockwood et al., 1999; Pastor et al., 2002; Scheffler et al., 1998; Talavage et al., 2000; Wessinger et al., 1997). In a PET study by Lockwood et al. (1999), 0.5-kHz tone bursts significantly activated volumes in the brainstem structures, in the medial geniculate nuclei, and bilaterally in the medial and lateral aspects of the superior temporal gyrus. Our results do not show the activation within the thalamus and brainstem because the sensitivity of MEG diminishes substantially with increasing depth. However, they are consistent with the location of activated cortex in the lateral superior temporal gyrus as reported by Lockwood et al. (1999). The broader cortical distribution reported by Lockwood et al. (1999) is most likely a result of PET being limited in its temporal resolution. These PET-activated volumes would include all AER

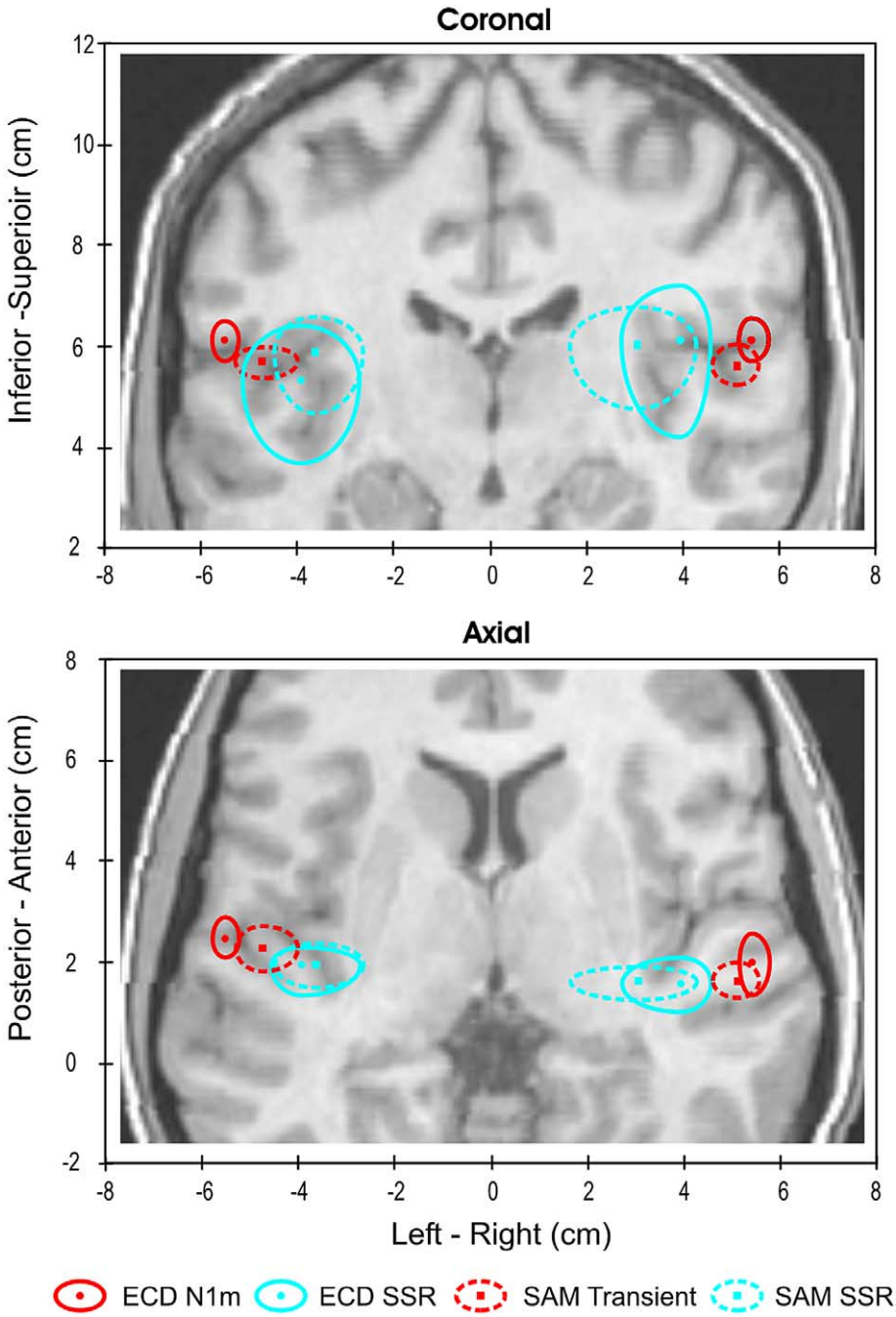

Fig. 4. Median locations and 95% confidence intervals of the SAM peak pseudo *t* values and dipoles (ECDs) for transient AERs and SSRs. The background coronal and axial slices are 2 cm anterior to and 6 cm superior to the center of the coordinate system, respectively.

components; for example, sustained activity would occur as a result of continuous presentation of the 500-ms tone bursts throughout the scanning period. Furthermore, fMRI studies have also shown this greater area of activation of the superior temporal gyrus (Belin et al., 1999; Bilecen et al., 1998; Scheffler et al., 1998; Talavage et al., 2000). Bilecen and colleagues (Bilecen et al., 1998; Scheffler et al., 1998) showed that 0.5-kHz and 1.0-kHz tone bursts activated structures along the entire length of Heschl's gyrus, including posterior–lateral regions of the superior temporal gyrus, which is a result of limited temporal resolution. Considering that the SAM results provide information of the timing of neural activity and that the SAM method can circumscribe the volume of cortical activity, the SAM approach has a clear advantage as compared to PET and fMRI.

For the SSRs, SAM images from single subjects show a volume of cortical activation in the medial aspect of the superior temporal gyrus. Although there is some variability between subjects, the SAM permutation results indicate a stable volume of activity across subjects. The active SAM volumes in the group after the permutation test include the medial aspect of Heschl's gyrus that spreads anteriorly.

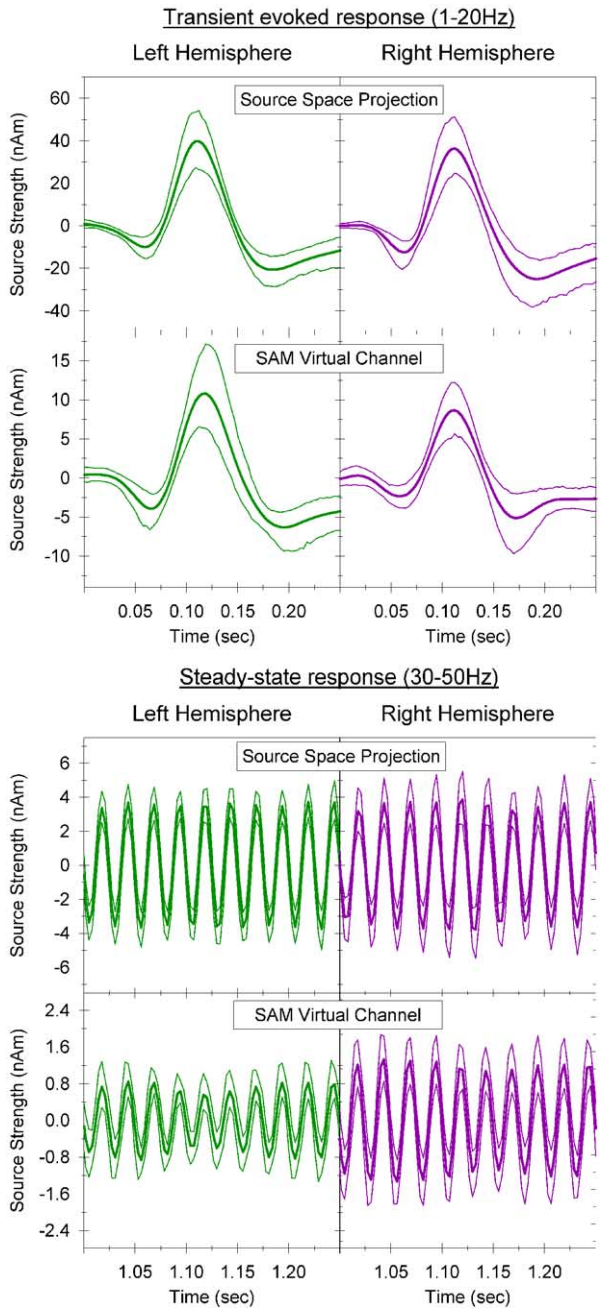

Fig. 5. Source activity analyzed using the source space projection and SAM virtual channel methods for transient AERs (top) and SSRs (bottom). Scales have been purposefully adjusted to the maximal response in order to make a visual comparison between the two analyses procedures (i.e., ECD and SAM). Thick lines represent the means of the response waveforms. Thin lines represent the bootstrap-sampled 95% confidence intervals.

Compared to the cytoarchitectonic description of the auditory cortex (Galaburda and Sanides, 1980), this active volume includes the medial koniocortex and the prokoniocortex. Auditory processing measured by changes in fMRI signals to low-frequency stimuli has also shown to be located within the region of the prokoniocortex (Talavage et al., 2000). Additionally, a PET study by Pastor et al. (2002) showed a broad region of activity in response to clicks presented at a rate of 40 Hz that was centerd over the medial koniocortex and extended into the prokoniocortex, which suggests the involvement of these areas in the processing of the auditory 40-Hz SSRs. Results from Pastor et al. (2002) are very similar to the present SAM permutation images for the 40-Hz SSRs. Albeit, it is possible that the extension of the activated volume into the prokoniocortex might be a result of localization error inherent in our methods and those in the fMRI and PET studies. However, it seems unlikely that all methods had a systematic error in the same anterior direction.

In contrast to the results of Pastor et al. (2002) showing cerebellar activity in response to 40-Hz steady-state stimuli, we found insufficient evidence to support this using SAM analysis. However, it might be difficult to use of MEG to resolve such an issue because the cerebellar neurons might be in a close-field distribution, are too deep, or are not tangentially oriented.

Because the 40-Hz SSRs are suggested to be predominantly generated in the primary auditory cortex (Pantev et al., 1993), which is approximately 2 cm in diameter, it might be possible that the extension into the prokoniocortex for 40-Hz SSRs is, to certain extent, a result of localization error. Such error may be due to head movement when recording MEG fields, variability in fiduciary points for coregistration between the MRI and MEG data, and variability in brain anatomy across subjects. We attempted to limit these sources of variability by excluding data from subjects whose head moved more than 8 mm in any direction within a recording block, using the same earpieces for the fiduciary markers in the MRI and MEG recordings, and normalizing each subject's MRI and SAM images into a common anatomical space.

As shown in Fig. 3, there seems to be a greater volume of activity for SSRs in the right than the left hemisphere. This result might suggest that there is greater propensity for neurons in the right hemisphere to process steady-state stimuli. However, 5 of 13 subjects had small pseudo t values (<1.5) for the left hemisphere as compared to only 3 subjects for the right. This variability in the data might contribute to the noticeable hemispheric asymmetry for SSRs and therefore further investigation is required.

Comparing the active SAM volumes between transient AERs and SSRs, it is clear that the transient AERs are generated by more laterally located structures in the superior temporal gyrus. Nonetheless, there is a small region of overlap between these volumes that lies in the transition boundary between the medial and lateral koniocortices. This suggests that neurons within this region might be involved in the generation of both the transient AERs and the SSRs. However, the SAM analysis for the transient AERs included the first 250 ms. Thus, the middle latency components (Pam-Nam-Pbm) within the first 50 ms after stimulus onset will have contributed to the gross activation, albeit small because they contribute less to the overall power spectrum used to calculate SAM images as compared to the long latency components (P1m-N1m-P2m). Assuming that there is some contribution from the middle latency components, the overlapping volumes between SSRs and transient AERs might come from the middle latency generators.

SAM vs ECD analyses

The SAM results of this study clearly demonstrate that the SAM approach can localize and differentiate between transient AER and SSRs within the auditory cortex. However, the question arises how consistent are the SAM results with respect to the well-established dipole modeling results, which have been obtained in series of EEG and MEG studies (cf. Eggermont and Ponton, 2002; Jacobson, 1994; Naatanen and Picton, 1987).

In order to compare the SAM and ECD results, we chose the location of the SAM voxel with the greatest (i.e., peak) pseudo *t* value to compare to the location of the ECD. The fact that there are no significant differences in locations of the sources between SAM and ECD analyses (see Fig. 4) suggests that SAM is as accurate at localizing cortical activity for the transient AERs as the ECD modeling. The N1m locations for ECD analysis from the present study are comparable to those reported previously in the MEG and EEG literature (Hari et al., 1980, 1987; Hari and Makela, 1986; Pantev et al., 1995; Pantev et al., 1993; Reite et al., 1981, 1994; Scherg and von Cramon, 1985). Spatiotemporal dipole modeling of the N1m shows that the center of gravity of its generator is within the lateral aspect of Heschl's gyrus, which corresponds to the lateral koniocortex (Kanno et al., 2001; Pantev et al., 1995; Reite et al., 1994; Yamamoto et al., 1988).

As compared to the locations of the SSR dipoles, SAM peak locations were not significantly different, which suggests that SAM can also localize the 40-Hz SSR as accurately as ECD modeling. Furthermore, ECD locations from the present study are comparable to previous studies showing that they are situated within the superior temporal gyrus (Bertrand et al., 1991; Herdman et al., 2002; Makela and Hari, 1987; Pantev et al., 1993, 1996; Romani, 1986). Pantev and colleagues coregistered these dipole locations onto subjects' MRIs and demonstrated they were in medial koniocortex (Pantev et al., 1996). We coregistered our dipole data with the subjects' MRIs and the results also support that 40-Hz SSR dipoles are located within the medial koniocortex.

Earlier research by Pantev and colleagues (1993) demonstrated that the 40-Hz SSR dipoles are clearly dissociable in space from the N1m dipoles. They reveal that the dipoles for the SSR are significantly more medially located than the dipoles for the N1m. In contrast, a study by Makela and Hari (1987) showed a nonsignificant difference between dipole locations of N1m and 40-Hz SSR. However, their results were based on a sample size of three, thereby limiting the power of their statistic. Contrary to this, our results from a larger sample size ($N = 13$) fully support the findings of Pantev et al. (1993). Median dipole locations for SSRs are significantly more medial than those for the N1m response, as indicated by nonoverlapping 95% confidence intervals. This suggests that generators of these components originate from separate cortical structures. However, the question of how spatially discrete the volumes of active neurons are is difficult to answer by means of ECD modeling. From the ECD results we can simply conclude that the centers of gravity for the N1m and SSRs are significantly separate. However, SAM can provide the volumetric information, which is certainly an advantage in imaging cortical activity.

Time domain

MEG fields

For all subjects, the field data reveal an onset response that has the prominent P1m-N1m-P2m peaks, as described previously (Elberling et al., 1980, 1982; Hari et al., 1980; Reite et al., 1981). However, it is difficult to compare the field data across subjects because differences in the head positioning with respect to the sensors. Therefore, we used the source space projection method to calculate the source waveforms, which can be then averaged across subjects.

SAM virtual channel vs source space projection

For the transient AERs, the SAM virtual channel waveform is similar in morphology to the source space projection waveform. They both show a triphasic waveform with peaks that are associated with the P1m-N1m-P2m complex seen in the field data. Thus, it is evident that the SAM virtual channel can extract the same temporal information for the transient AER sources, as compared to the source space projection method. This is also true for the 40-Hz SSRs, which is consistent with the 40-Hz oscillations of tangentially oriented cortical sources as reported by Herdman et al. (2002). Our SAM results indicate smaller 40-Hz source strengths in the left hemisphere than the right hemisphere for the SAM virtual channel. However, this difference is not significant and can be explained by the scaling factor that is chosen to view the results. The scale is adjusted for the SAM virtual channel to match the same height of the source space projection data for simple comparison of the waveforms across measures. The 95% confidence intervals, shown in Fig. 5, reveal that between left and right hemispheres the intersubject variability in the SAM virtual channels is similar to the variability in the source space projection waveforms. The overlap of the confidence intervals between hemispheres indicates that there are no significant differences.

Conclusion

Results from the present study indicate that the SAM method can accurately localize transient AERs and 40-Hz SSR in both space and time. Furthermore, it is sensitive enough to dissociate these functionally discrete brain volumes.

Acknowledgments

Grants from the Canadian Institutes of Health Research and the Rotman Research Institute supported this research project.

References

Barnes, G.R., Hillebrand, A., 2003. Statistical flattening of MEG beamformer images. Hum. Brain Mapp. 18 (1), 1–12.

Belin, P., Zatorre, R.J., Hoge, R., Evans, A.C., Pike, B., 1999. Event-related fMRI of the auditory cortex. Neuroimage 10 (4), 417–429.

Bertrand, O., Perrin, F., Pernier, J., 1991. Evidence for a tonotpic organization of the auditory cortex observed with auditory evoked potentials. Acta Otolaryngol. Suppl. 491, 116–123.

Bilecen, D., Scheffler, K., Schmid, N., Tschopp, K., Seelig, J., 1998. Tonotopic organization of the human auditory cortex as detected by BOLD-fMRI. Hearing Research 126, 19–27.

Cohen, L.T., Rickards, F.W., Clark, G.M., 1991. A comparison of steady-state evoked potentials to modulated tones in awake and sleeping humans. J. Acoust. Soc. Am. 90, 2467–2479.

Eggermont, J.J., Ponton, C.W., 2002. The neurophysiology of auditory perception: from single units to evoked potentials. Audiol. Neuro-Otology 7 (2), 71–99.

Elberling, C., Bak, C., Kofoed, B., Lebech, J., Saermark, K., 1980. Magnetic auditory responses from the human brain. Scand. Audiol. 9, 185–190.

Elberling, C., Bak, C., Kofoed, B., Lebech, J., Saermark, K., 1982. Auditory magnetic fields. Scand. Audiol. 11, 61–65.

Galaburda, A., Sanides, F., 1980. Cytoarchitectonic organization of the human auditory cortex. J. Comp. Neurol. 190, 597–610.

Galambos, R., Makeig, S., Talmachoff, P., 1981. A 40-Hz auditory potential recorded from the human scalp. Proc. Natl. Acad. Sci. USA 78 (4), 2643–2647.

Gutschalk, A., Mase, R., Roth, R., et al., 1999. Deconvolution of 40 Hz steady-state fields reveals two overlapping source activities of the human auditory cortex. Clin. Neurophysiol. 110 (5), 856–868.

Hamalainen, M., Hari, R., Ilmoniemi, R.J., Knuutila, J., Lounasmaa, O.V., 1993. Magnetoencephalography—theory, instrumentation, and applications to noninvasive studies of the working human brain: review. Mod. Phys. 65 (2), 413–496.

Hari, R., Aittoniemi, K., Jarvinen, M.-L., Katila, T., Varpula, T., 1980. Auditory evoked transient and sustained magnetic fields of the human brain. Exp. Brain Res. 40, 237–240.

Hari, R., Hamalainen, M., Joutsiniemi, S., 1989. Neuromagnetic steady-state responses to auditory stimuli. J. Acoust. Soc. Am. 86, 1033–1039.

Hari, R., Makela, J.P., 1986. Neuromagnetic responses to frequency modulation of a continuous tone. Acta Oto-Laryngol. Suppl. 432, 26–32.

Hari, R., Pelizzone, M., Makela, J.P., et al., 1987. Neuromagnetic responses of the human auditory cortex to on- and offsets of noise bursts. Audiol. 26 (1), 31–43.

Herdman, A.T., Lins, O., Van Roon, P., et al., 2002. Intracerebral sources of human auditory steady-state responses. Brain Topogr. 15 (2), 69–86.

Ilmoniemi, R.J., Williamson, S.J., Hostetler, W.E., 1987. New method for the study of spontaneous brain activity. in: Williamson, S.J. (Ed.), Biomagnetism. Tokyo Denki University Press, Tokyo, pp. 182–185.

Ishii, R., Shinosaki, K., Ukai, S., et al., 1999. Medial prefrontal cortex generates frontal midline theta rhythm. NeuroReport 10 (4), 675–679.

Jacobson, G.P., 1994. Magnetoencephalographic studies of auditory system function. J. Clin. Neurophysiol. 11 (3), 343–365.

Johnsrude, I.S., Giraud, A.L., Frackowiak, R.S., 2002. Functional imaging of the auditory system: the use of positron emission tomography. Audiol. Neuro-Otol. 7 (5), 251–276.

Kanno, A., Nakasato, N., Murayama, N., Yoshimoto, T., 2001. Middle and long latency peak sources in auditory evoked magnetic fields for tone bursts in humans. Neurosci. Lett. 293, 187–190.

Lockwood, A.H., Salvi, R.J., Coad, M.L., et al., 1999. The functional anatomy of the normal human auditory system: responses to 0.5 and 4.0 kHz tones at varied intensities. Cereb. Cortex 9 (1), 65–76.

Makela, J.P., Hari, R., 1987. Evidence for cortical origin of the 40 Hz auditory evoked response in man. Electroencephalogr. Clin. Neurophysiol. 66, 539–546.

Naatanen, R., Picton, T., 1987. The N1 wave of the human electric and magnetic response to sound: a review and an analysis of the component structure. Psychophysiology 24 (4), 375–425.

Pantev, C., 1995. Evoked and induced gamma-band activity of the human cortex. Brain Topogr. 7 (4), 321–330.

Pantev, C., Bertrand, O., Eulitz, C., et al., 1995. Specific tonotopic organizations of different areas of the human auditory cortex revealed by simultaneous magnetic and electric recordings. Electroencephalogr. Clin. Neurophysiol. 94 (1), 26–40.

Pantev, C., Elbert, T., Makeig, S., et al., 1993. Relationship of transient and steady-state auditory evoked fields. Electroencephalogr. Clin. Neurophysiol. 88 (5), 389–396.

Pantev, C., Gallen, C., Hampson, S., Buchanan, S., Sobel, D., 1991a. Reproducibility and validity of neuromagnetic source localization using a large array biomagnetometer. Am. J. EEG Technol. 31, 83–101.

Pantev, C., Hoke, M., Lutkenhoner, B., Lehnertz, K., 1991b. Neuromagnetic evidence of functional organization of the auditory cortex in humans. Acta Otolaryngol. Suppl. 491, 106–114.

Pantev, C., Roberts, L.E., Elbert, T., Ross, B., Wienbruch, C., 1996. Tonotopic organization of the sources of human auditory steady-state responses. Hear. Res. 101 (1–2), 62–74.

Pastor, M.A., Artieda, J., Arbizu, J., et al., 2002. Activation of human cerebral and cerebellar cortex by auditory stimulation at 40 Hz. J. Neurosci. 22 (23), 10501–10506.

Picton, T.W., Hillyard, S.A., Krausz, H.I., Galambos, R., 1974. Human auditiory evoked potentials. I. Evaluation of components. Electroencephalogr. Clin. Neurophysiol. 36, 179–190.

Reite, M., Adams, M., Simon, J., et al., 1994. Auditory M100 component 1: relationship to Heschl's gyri. Cogn. Brain Res. 2 (1), 13–20.

Reite, M., Zimmerman, J.T., Zimmerman, J.E., 1981. Magnetic auditory evokde fields: interhemispheric asymetry. Electroencephalogr. Clin. Neurophysiol. 51, 388–392.

Robinson, S.E., 1989, Theory and properties of lead field synthesis analysis, in: Williamson, S., Hoke, M., Struink, G., Kotani, M. (Eds.), Advances in Biomagnetism, Plenum Press, pp. 599–602.

Robinson, S.E., Rose, D.F., 1992. Current source image estimation by spatially filtered MEG. in: Romani, G. (Ed.), Biomagnetism: Clinical Aspects. Excerpta Medica, Amsterdam, pp. 761–765.

Robinson, S.E., Vrba, J., 1998. Functional neuroimaging by synthetic aperture magnetometry (SAM). in: Yoshimoto, T., Kotani, M., Kuriki, S., Karibe, H., Nakasato, N. (Eds.), Recent Advances in Biomagnetism. Tohuku University Press, Sendai, pp. 302–305.

Romani, G.L., 1986. Tomotopic organization of the human auditory cortex revealed by steady state neuromagnetic measurements. Acta Otolaryngol. Suppl. 432, 33–34.

Ross, B., Picton, T.W., Pantev, C., 2002. Temporal integration in the human auditory cortex as represented by the development of the steady-state magnetic field. Hearing Res. 165 (1-2), 68–84.

Scheffler, K., Bilecen, D., Schmid, N., Tschopp, K., Seelig, J., 1998. Auditory cortical responses in hearing subjects and unilateral deaf patients as detected by functional magnetic resonance imaging. Cereb. Cortex 8 (2), 156–163.

Scherg, M., von Cramon, D., 1985. Two bilateral sources of the late AEP as identified by a spatio-temporal dipole model. Electroencephalogr. Clin. Neurophysiol. 62, 32–44.

Singh, K.D., Barnes, G.R., Hillebrand, A., Forde, E.M., Williams, A.L., 2002. Task-related changes in cortical synchronization are spatially coincident with the hemodynamic response. NeuroImage 16 (1), 103–114.

Talavage, T.M., Ledden, P.J., Benson, R.R., Rosen, B.R., Melcher, J.R., 2000. Frequency-dependent responses exhibited by multiple regions in human auditory cortex. Hear. Res. 150 (1–2), 225–244.

Taniguchi, M., Kato, A., Fujita, N., et al., 2000. Movement-related desynchronization of the cerebral cortex studied with spatially filtered magnetoencephalography. NeuroImage 12 (3), 298–306.

Van Veen, B.D., van Drongelen, W., Yuchtman, M., Suzuki, A., 1997. Localization of brain electrical activity via linearly constrained minimum variance spatial filtering. IEEE Transact. Biomed. Engineer. 44 (9), 866–880.

Wessinger, C.M., Buonocore, M.H., Kussmaul, C.L., Mangun, G.R., 1997. Tonotopy in human auditory cortex examined with functional magnetic resonance imaging. Brain Mapp. 5, 18–25.

Yamamoto, T., Williamson, S.J., Kaufman, L., Nicholson, C., Llinás, R., 1988. Magnetic localization of neuronal activity in the human brain. Proc. Natl. Acad. Sci. USA 85, 8732–8736.